AD_____

Award Number:
W81XWH-09-1-0661

TITLE:
Intraoperative Molecular Imaging for Rapid Assessment of Tumor Margins

PRINCIPAL INVESTIGATOR:
Scott C. Davis

CONTRACTING ORGANIZATION:

Dartmouth College

Hanover, NH 03755

REPORT DATE:
September 2010

TYPE OF REPORT:
Annual summary report

PREPARED FOR: U.S. Army Medical Research and Materiel Command
Fort Detrick, Maryland 21702-5012

DISTRIBUTION STATEMENT:

☑ Approved for public release; distribution unlimited

REPORT DOCUMENTATION PAGE

Form Approved
OMB No. 0704-0188

1. REPORT DATE *(DD-MM-YYYY)*	**2. REPORT TYPE**	**3. DATES COVERED** *(From - To)*
01-09-2010	Annual summary report	1 SEP 2009 - 31 AUG 2010

4. TITLE AND SUBTITLE
Intraoperative Molecular Imaging for Rapid Assessment of Tumor Margins

5a. CONTRACT NUMBER

5b. GRANT NUMBER
W81XWH-09-1-0661

c. PROGRAM ELEMENT NUMBER

6. AUTHOR(S)
Scott C. Davis

5d. PROJECT NUMBER

5e. TASK NUMBER

5f. WORK UNIT NUMBER

7. PERFORMING ORGANIZATION NAME(S) AND ADDRESS(ES)
Dartmouth College
Hanover, NH 03755

8. PERFORMING ORGANIZATION REPORT

9. SPONSORING / MONITORING AGENCY NAME(S) AND ADDRESS(ES)
U.S. Army Medical Research and Materiel Command
Fort Detrick, Maryland 21702-5012

10. SPONSOR/MONITOR'S ACRONYM(S)

11. SPONSOR/MONITOR'S REPORT NUMBER(S)

12. DISTRIBUTION / AVAILABILITY STATEMENT
Approved for public release; distribution unlimited

13. SUPPLEMENTARY NOTES

14. ABSTRACT

The objective of this research is to develop methods for rapid detection of tumor margins during breast cancer surgery using targeted fluorescence-labeled tracers. Three dimensional modeling of tumors in excised tissue has be en accomplished and the introduction of spectral resolution in the imaging strategy shows promise for quantifying tumor depth in the tissue. A spectrally-resolved prototype imaging system was developed and initial studies demonst rated the potential to determine the depth of embedded tumor fragments in the excise tissue or surgical cavity. Pilot animal data with the Licor IRDye800CW-2DG imaging agent in excised MDA231 tumors showed poor specificity and tumor penetration , though further studies with more specific probes are ongoing. Finally, ROC analysis quantified the improvement in diagnostic performance of diffuse tomography when accurate MRI information is encoded in the imaging algorithm.

15. SUBJECT TERMS
fluorescence, molecular imaging, surgery, breast cancer, fluorescence guided surgery, animal models

16. SECURITY CLASSIFICATION OF:			**17. LIMITATION OF ABSTRACT**	**18. NUMBER OF PAGES**	**19a. NAME OF RESPONSIBLE PERSON USAMRMC**
a. REPORT	**b. ABSTRACT**	**c. THIS PAGE**			**19b. TELEPHONE NUMBER** *(include area code)*
U	U	U	UU	37	

Standard Form 298 (Rev. 8-98)
Prescribed by ANSI Std. Z39.18

Table of Contents

Page

Introduction

The scientific objective of this research is to explore the feasibility of assessing tumor status during breast cancer surgery using targeted fluorescence-labeled tracers. Under normal surgical conditions, surgeons rely on gross examination of the surgical cavity and the excised tissue to help guide the extent of tissue removal. Post-surgical analysis using thin slices of tissue stained for physiochemical features is required to provide definitive assessments of the distance between tumor tissue and the edge of the excised tissue, also known as tumor margin. The tumor margin status has a significant impact on the risk of cancer recurrence, and a diagnosis of "narrow" or "involved" margins requires the patient to return for additional surgical resection. Rates of repeat surgeries to clear tumor tissue are surprisingly high, approaching 50% for the patient population undergoing breast-conserving surgery for ductal carcinoma in situ (DCIS), a type of breast cancer that has yet to become invasive. We hypothesize that targeted fluorescent drugs coupled with an appropriate, rapid fluorescence imaging system will inform the surgeon or surgical pathologist of tumor margin status in excised specimens during the surgical procedure. Eliminating the need to inject or otherwise administer the drug to the patient would allow the use of fluorophores that do not have proven safety profiles, thus removing a large barrier to widespread adoption of the procedure in clinical practice. The project involves numerical modeling of light propagation to design an optimized surgical specimen scanner, animal experiments to investigate the behavior of different targeted fluorophores applied topically to the tissue specimens, and a pilot study with human tissue in the later stages of the project. Ultimately, it is our hope that information provided by this imaging reduces re-excision rates.

Body

Progress has been made toward the proposed aims of this project including development of light propagation models for assessing tumor margin status (Task 3), design and development of an experimental imaging system (Task 3), imaging of ex-vivo tissues from animal models (Tasks 1 and 2), and modeling data to assess sensitivity and specificity metrics of imaging in vivo (Task 4). A description of the primary accomplishments and ongoing efforts follows.

Light propagation modeling and diagnostic

A critical aim of the project is to determine feasibility of detecting tumor margins in excised tissue during surgery. Toward that end, we have developed sophisticated light modeling algorithms to simulate the light propagation in sections of tissue encountered during surgery. These algorithms are part of the NIRFAST software package which is a finite element-based method package based on the diffusion approximation of photon propagation in tissue. Originally developed for in vivo imaging in relatively large tissue volumes, this software has been modified to investigate reflectance-mode fluorescence imaging for surgical settings as part of this project. Accurate light modeling of tissue sections allows optimization of the intra-surgical imaging system.

Figure 1 illustrates the modeling capabilities developed. A simulated test domain was creating from an archive photograph of a breast tissue section (Fig. 1 (a)). By estimating a tissue thickness, the 2-D outline of the tissue from the photograph was used to generate a 3-D finite element mesh of 46,000 nodes. Four simulated tumor fragments were added to the simulated tissue volume at different depths from the tissue surface. Semi-transparent surface renderings containing interior cross sections in two different planes to show the location and shapes of the simulated tumor regions are presented in Figs. 1(b) and (c). In this example, tumor-to-background fluorescence intensity was assumed to be 20:1 for all four fragments. Figure 2 (d) shows the simulated illumination intensity of the excitation source on the tissue surface, modeled as a dense grid of point sources. This excitation illumination induces fluorescence throughout the tissue volume. The remitted fluorescence is shown in Fig. 2(e), and represents what the surgeon would see

under these conditions. Most tumor fragments generate substantial fluorescence contrast on the surface. The small fragment buried further in the tissue is not detectable.

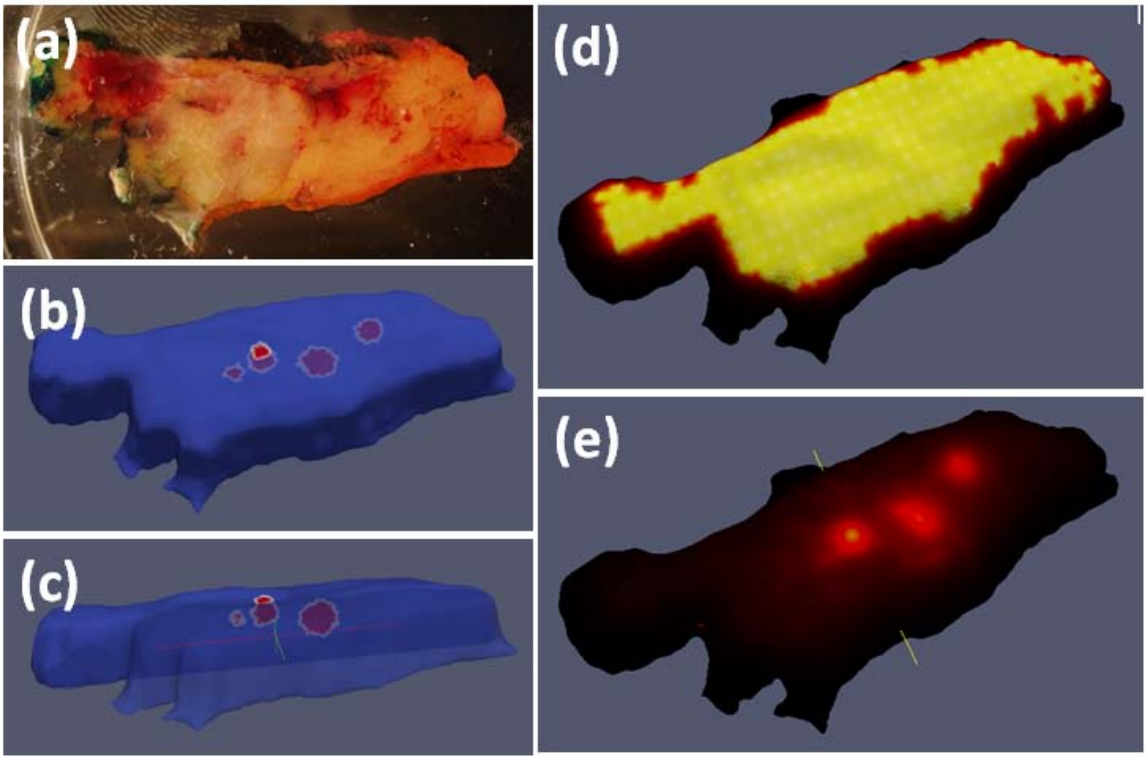

Figure 1. An archive photo of a tissue specimen in (a) was used to generate a finite element mesh containing simulated tumor fragments shown in (b) and (c). The remitted fluorescence from the tumor tissue excited by an illumination source shown in (d) is presented in (e).

Spectrally resolved wide-field imaging for assessing tumor depth

The ability to quickly determine tumor depth from the tissue surface either in a fresh specimen or in a surgical cavity may benefit efforts to reduce patient callback after breast surgery. One approach towards quantify tumor depth is to take advantage of the spectral distortion of the fluorescence peak as it propagates through tissue (*1-3*). This is due to the spectral variation of optical properties. Fluorescence from deeper tumors will be distorted to a greater degree than those near the surface, and it may be possible to exploit this phenomenon to provide an estimate of depth that is clinically relevant.

The simulated experiment in Fig. 2 demonstrates the spectral distortion of an embedded tumor. The large gray region represents a 2-D cross section of tissue with the sources aligned along the top of the region. These sources were assumed to be illuminated simultaneously to represent a broad-beam imaging system. A simulated tumor with 10:1 contrast to the background is shown at a relatively deep position within the tissue. In this study, the depth of this tumor was varied over a range of about 18mm, as illustrated in the figure. At each depth, the spectrum of the emitted fluorescence was calculated for discrete positions on the tissue surface. These spectra are shown in the figure. Obviously, spectra far from the position of the tumor are not affected noticeably by the changing depth. Near the tumor the overall intensity of the remitted fluorescence changes dramatically with depth and there is a noticeable change in the shape of the spectrum.

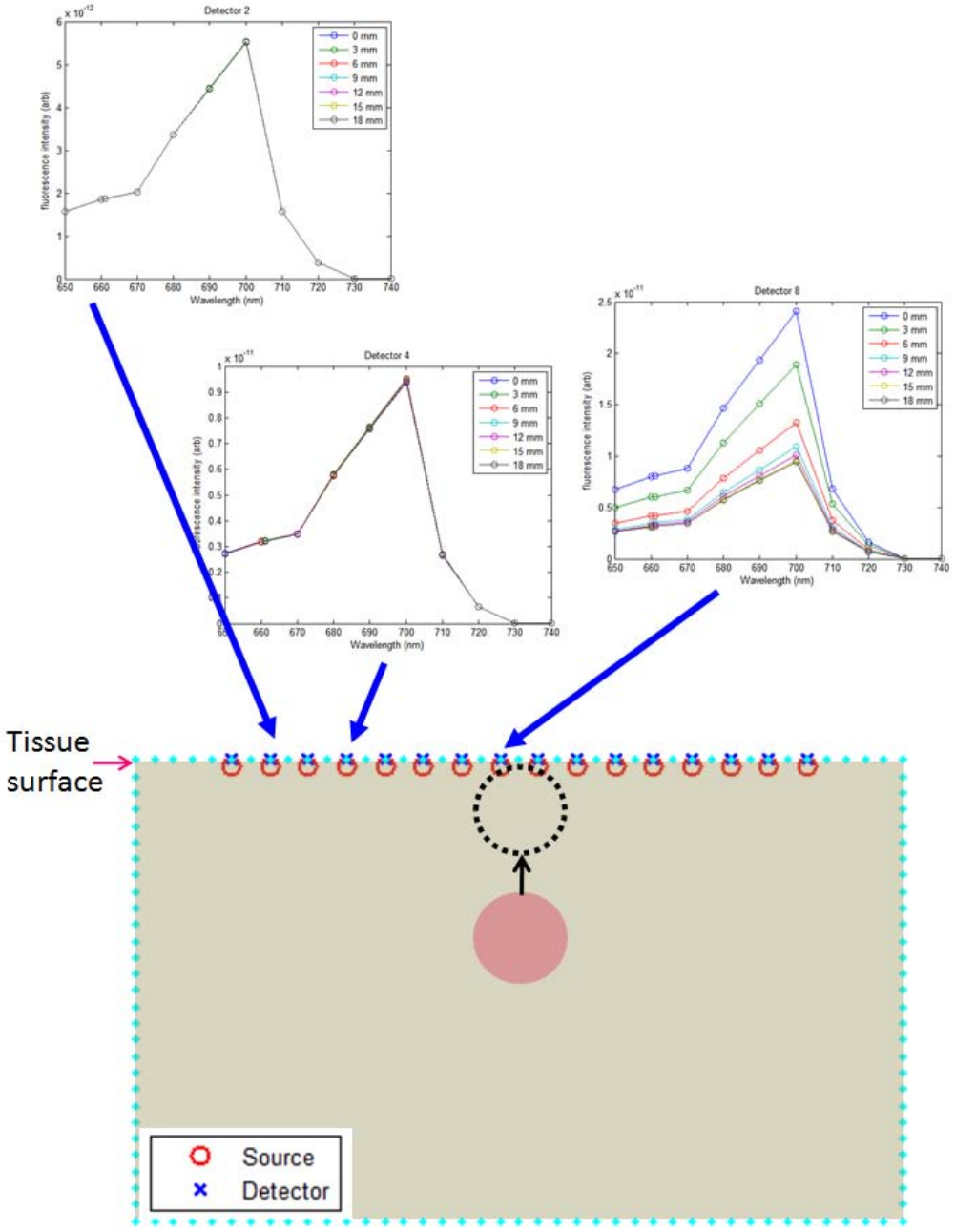

Figure 2. Three fluorescence spectra remitted from the tissue at different spatial points are shown above the blue arrows. The depth of the simulated tumor mass was varied, as can be seen in the cross-sectional view of the tissue in gray. For points on the tissue surface near the tumor, the remitted fluorescence spectra change noticeably with changing tumor depth

A simple ratio between two wavelengths may provide depth information. Figure 3 shows the same domain, again illustrating different positions of the same tumor as in Fig. 2, above which is reported the ratio of two wavelengths in the emission spectrum resolved spatially. Changes in the ratio correspond to changes in depth, however, the ratiometric measurement is not unique with depth. Other factors, such as relative position on the tissue surface, size of the tumor, and contrast will all play a role in the ratio value. However, if a few of these parameters can be assumed, which is feasible, it may be possible to decrease the

non-uniqueness of the problem. This is part of ongoing work on this project.

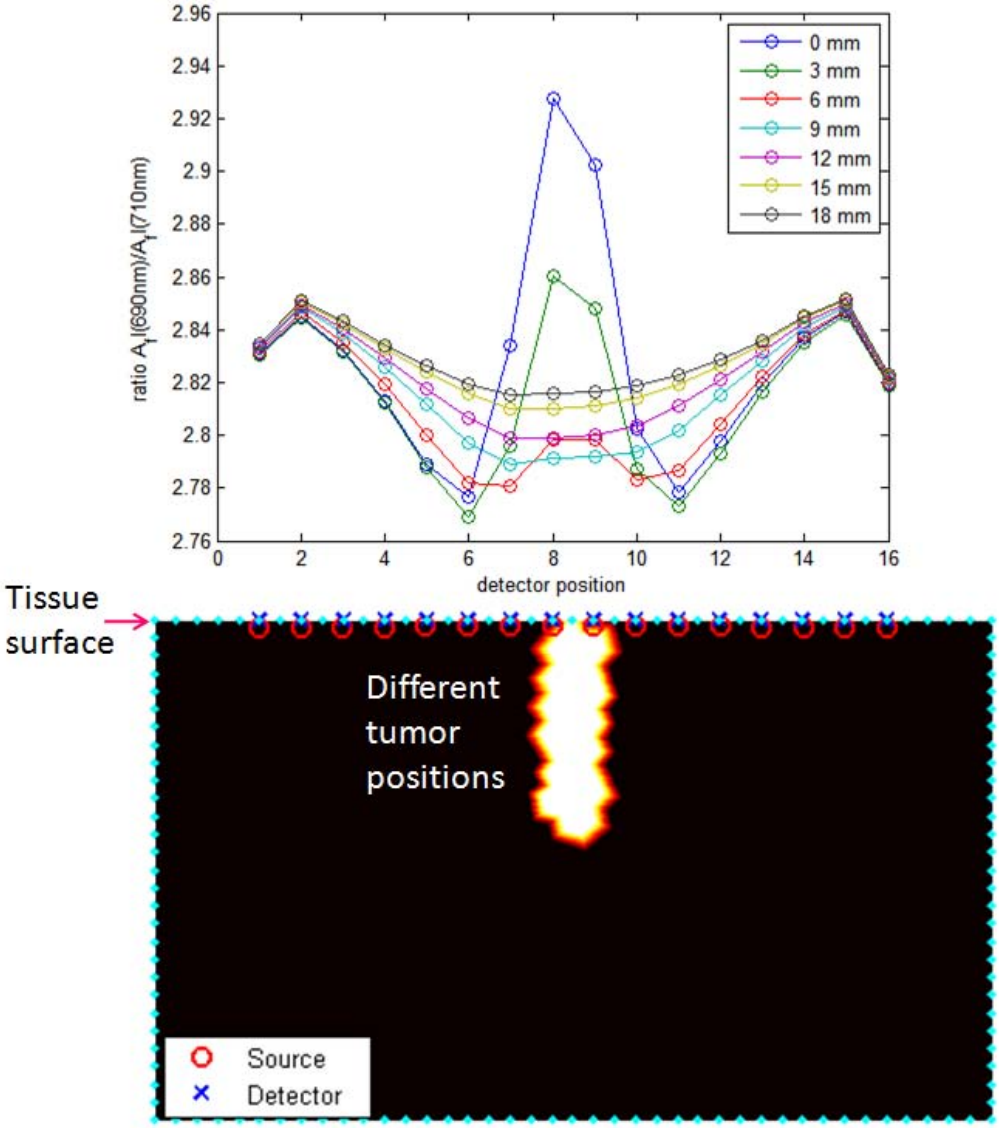

Figure 3. The ratios of two wavelengths in the emission spectrum of the fluorophore are plotted for different points on the tissue surface. The white blotches within the black diagram illustrate the different tumor positions. Detector positions on the tissue surface correspond to the ratio plot directly above.

We have also developed an innovative mathematical technique to estimate depth based on analytical solutions to the diffusion equation. This simplification is also based on ratiometric measurements at different wavelengths but has significant computational efficiency advantages over numerical approaches and therefore can be integrated easily and calculated at higher rates than video. Please refer to the attached paper for details. While the paper focuses on a specific organ region (brain tumor surgery in this example), the technique is generic in its application and can readily be applied to any organ.

Finally, we are currently working to integrate more accurate light propagation models, such as Monte

Carlo simulations for irregular domains, into the software package. These models will provide a more accurate representation of what the surgeon will see with an intra-surgical imaging system and thus allow further refinement of these system configurations.

Imaging system design

An initial experimental assessment of the analytical ratiometric method for determining tumor depth has been performed by designing an instrument for wide-field acquisition of multi-spectral measurements, as shown in Fig. 4. In this experiment, fluorescence excitation was done using an expanded beam of a diode laser with wavelength λ^{ex} = 635 nm (Power Technology Inc., Little Rock, Arkansas). Remitted fluorescence was measured at five wavelengths, λ = (675, 685, 695, 705, 715) nm, using 10 nm-wide band-pass interference filters (Omega Optical, Brattleboro, Vermont) inserted into a motorized wheel coupled to an EXi Aqua charge-coupled device (CCD) (QImaging, Surrey, British Columbia). The camera was cooled at 0°C and has a full well-depth of 18,000 e-, a 14 bits digitizer, a dark current of 0.15 e-/pixel/seconds and a read-noise of 6.5 e- when operated at 10MHz readout frequency.

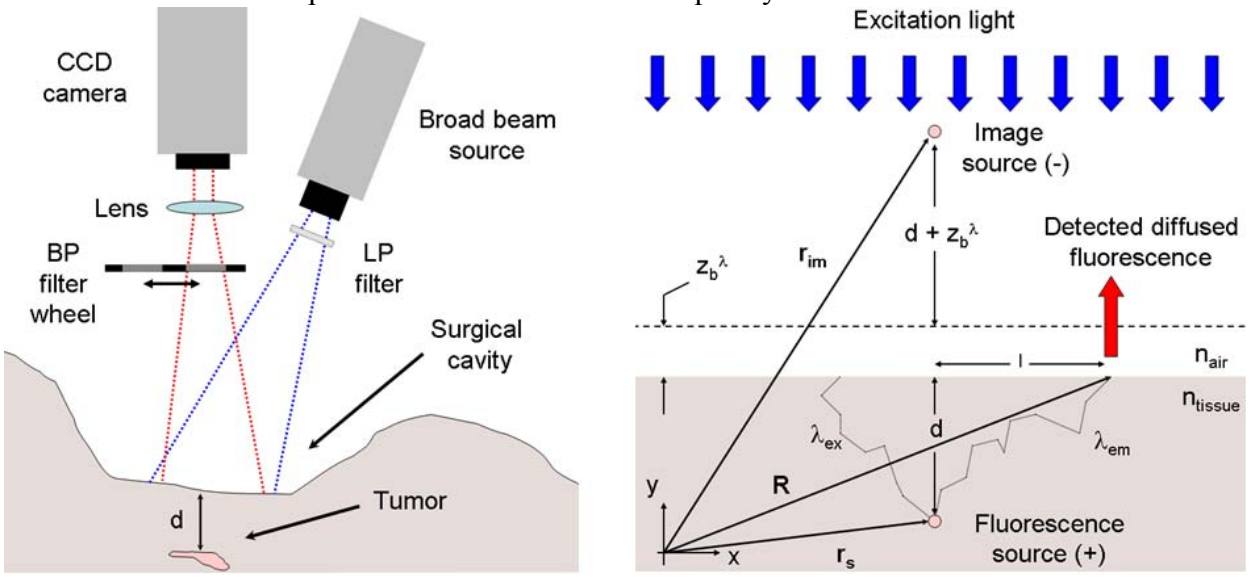

Figure 4. (a) Non-contact multi-spectral imaging instrument used for fluorescence-ratio detection. (b) Light transport is modeled assuming the cavity can be approximated as a semi-infinite diffusive medium with homogeneous optical properties.

This system was used to test the analytical ratiometric methodology by imaging a tissue-simulating blood phantom with protoporphyrin IX as a fluorophore. A container (dimensions: 150 mm × 75 mm × 61 mm) was filled with water containing a volume fraction of 1 % in tralipid (Baxter Healthcare Corp., Deerfield, Illinois) and 2% porcine blood. An optically transparent cylindrical inclusion (diameter: 5.5 mm, height: 10 mm) was filled with 20 μg/ml of PpIX (Frontier Scientific, Logan, Utah) dissolved in dimethyl sulfoxide (DMSO). A moving stage allowed the simulated tumor to be immersed at different depths. The medium was illuminated using an expanded laser beam (diameter: 13 mm, P = 5.5 mW, λ^{ex} = 635 nm). Fluorescence images at five different wavelengths were acquired (d = 1 to 15 mm). A PpIX spectrum was acquired to be used as a reference that was not corrupted by light propagation in the medium. Associated with each fluorescence image, a pre-contrast image (inclusion filled with DMSO only) was acquired and subtracted from the corresponding image to account for excitation light filter bleed-through. Fig. 5(b)

shows the measured ratios for two sets of wavelengths: (λ_1, λ_2) = (675 nm, 685 nm) (circles) and (λ_1, λ_2) = (675 nm, 695 nm) (squares). The dotted lines correspond to simulated ratios computed with the analytical approximation using the optical properties experimentally retrieved with a fiber-optics probe (Fig. 5(a)). Qualitative inspection of the data suggests a reasonable match between theory and experiment, although a significant level of noise is observed mainly due to excitation light filter bleed-through, limited light power delivered to the tissue surface and variations of the optical properties of the blood phantom during the experiment (as much as 20% for the absorption coefficient). Using a (non-parametric) Spearman's rank correlation test a significant correlation was found between the experimental data and the theoretical predictions. The correlation coefficients and P-values obtained were $r_s = 0.90$, $P = 0.0046$ (two-tailed) for (λ_1, λ_2) = (675 nm, 685 nm) and $r_s = 0.83$, $P = 0.015$ (two-tailed) for (λ_1, λ_2) = (675 nm, 695 nm). A linear regression was performed on the data with goodness-of-fit parameters $r^2 = 0.84$ and $r^2 = 0.64$ for (λ_1, λ_2) = (675 nm, 685 nm) and (λ_1, λ_2) = (675 nm, 695 nm), respectively. Another statistical analysis (F-test) was performed to test for the presence of a non-zero slope in the relationship between Γ and d. We found that for both sets of wavelengths the data was significantly different from a horizontal line ($P<0.05$).

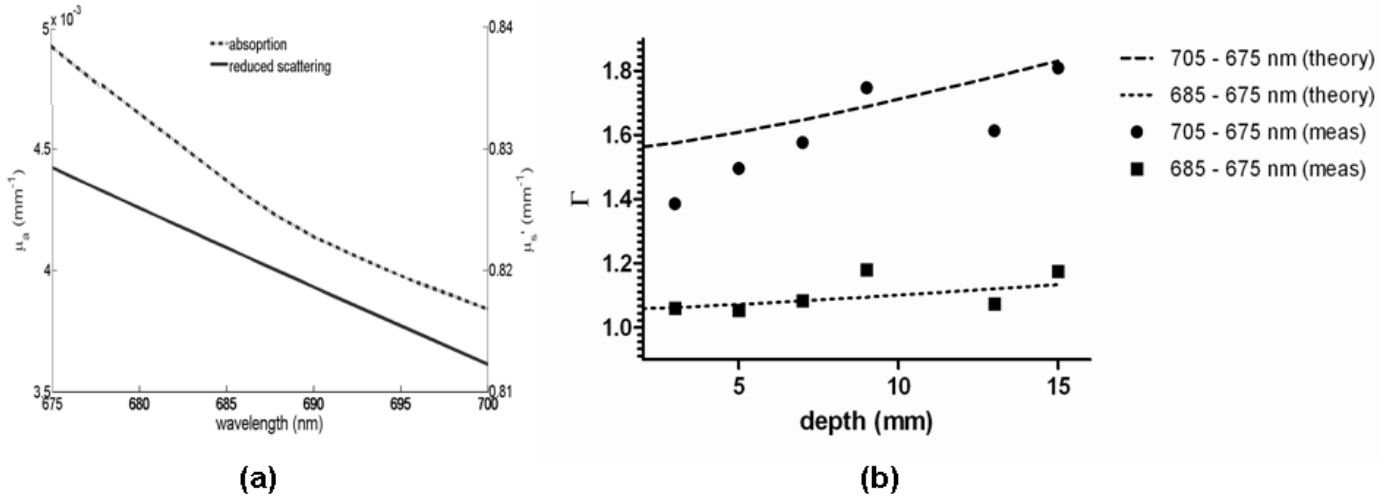

Figure 5. Experimental data acquired using a tissue-simulating phantom: (a) Optical properties (absorption and reduced scattering) measured with the a fiber probe, (b) Simulated (theory) versus measured (meas) fluorescence ratios for two sets of wavelengths showing correlation with depth.

Animal experiments

In collaboration with Dr. Hoopes's lab, excised tissue from a small number (N=4) of animals was imaged on the Licro Odyssey specimen scanner. After tumors reached approximately 7 mm across, the animals were sacrificed and the tumor immediately removed with adjacent normal tissue. All tissue were soaked for 5 – 20 minutes in a solution of Licor IRDye800CW-2DG and then rinsed for 5 – 20 minutes in a PBS solution. The tissues were then scanned on the fluorescence scanner and white light photos taken without changing the geometry of the specimens. Figure 6 shows the white light and fluorescence image pairs for specimens taken from two animals. The two central images in (d) are of a cross-section of the tumor slices in two after being soaked and rinsed. These images indicate that the drug does not appear to penetrate the tumor well and normal tissue uptake, or autofluorescence, seems to be significant with this drug. These preliminary results suggest that this optical probe may not have the specificity required for margin detection; however, further examination is required to be conclusive.

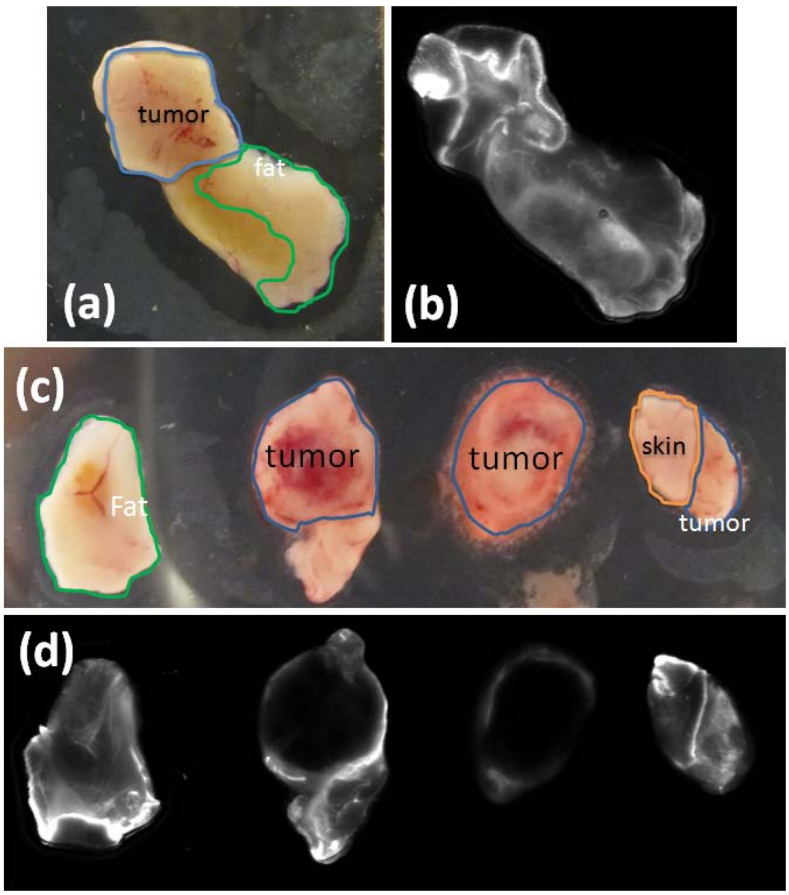

Figure 6. White light images and corresponding fluorescence images for tumors excised from two animals ((a) and (b) for one animal and (c) and (d) for the second). In (c), the central two specimens are the same tumor sliced down the middle after soaking in Licor IRDye800CW-2DG, showing a cross section of the tumor mass. These images show a significant amount of non-specific uptake of the probe in normal tissue and poor penetration into the tumor mass.

Working with Dr. Hoopes, Dr. Julia O'hara and their colleagues, I have gained experience in the methods used to implant breast cancer tumor lines in the mammary fat pad of nude mice. As the study has progressed, we have switched from the SKBR-3 breast cancer line to a HER2/neu positive BT474 and MDA231 (HER2/neu negative) which we have found grow more readily in vivo. The use of a negative control is an important addition to the study design. Currently, we have 40 animal subjects growing breast cancer tumor models for this project, 20 with HER2/neu positive BT474 tumors and 20 with MDA231 cells. Implantations were performed with 5 x 10^6 cells in matrigel. Estrogen pellets were also implanted under the skin of mice inoculated with BT474 cells to promote tumor growth. Tumors in these populations should be mature within 1 – 2 months from the date of this report.

Assessment of diagnostic performance of optical imaging of breast cancer in vivo

One component of the project involves in vivo assessment of breast using MRI-guided fluorescence molecular tomography. In this paradigm, tissue region segmented out of the simultaneously acquired MR images is used to guide the diffuse optical image reconstruction process. While MRI-coupled optical tomography has matured over the past decade, the benefits of incorporating MRI structural information in the image recovery of optical properties has not been quantified beyond anecdotal case studies. In this

study, the improvements of MRI priors over standard diffuse imaging without spatial guidance are quantified in terms of diagnostic performance. A simulated breast volume made up of fatty, fibro-glandular and tumor regions was used as the test domain. A range of tumor sizes and contrasts, including MRI false positive cases, were simulated and images were recovered with or without the use of the MRI spatial prior information. Receiver Operating Characteristic (ROC) analysis was used to quantify diagnostic performance of each technique. The results are shown in Fig. 7 for ROC analysis performed without MRI guidance, with MRI priors assuming that the internal structure is accurate, and with MRI priors assuming that the internal structure of the fibro-glandular tissue is incorrectly dilated by 1 pixel, for (a), (b), and (c), respectively. Area-under-the-curve (AUC) values are 0.73, 0.85, and 0.75, respectively, indicating that the use of MRI priors improves diagnostic performance, provided the internal structure obtained from the modality is accurate. Further analysis is ongoing.

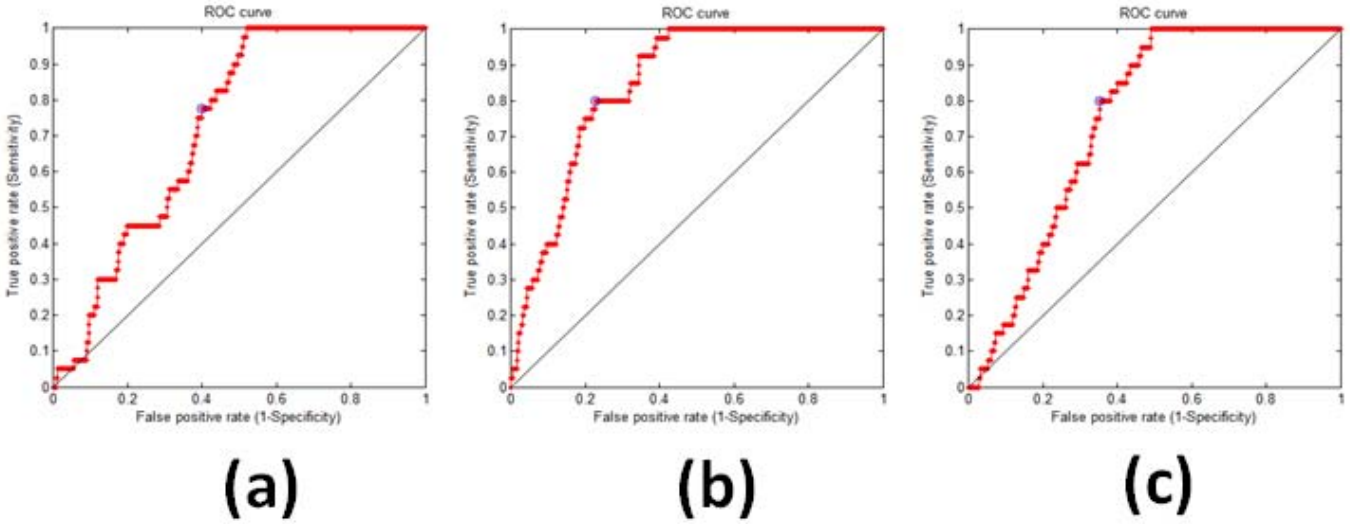

Figure 7. ROC curves for diagnostic performance of standard diffuse tomography, (a), image-guided diffuse tomography assuming accurate structural priors, (b), and image-guided diffuse tomography assuming inaccurate structural priors, (c).

Key research accomplishments

- Developed modeling algorithms for simulating imaging of fresh, excised tissue and the surgical cavity.
- Developed a method for identifying depth of tumors from the tissue surface in a surgical setting. This technique is applicable to tissue volumes in the surgical cavity or fresh, excised tissue.
- Contributed to the design, construction, and experimental validation of a spectrally-resolved intra-surgical imaging system.
- Acquired preliminary data in a small number of animals to demonstrate penetration of targeted fluorescence probe in fresh excised tissue. Initial readings do not show a high level of specificity or penetration depth with this optical probe.
- Assessed diagnostic performance of MRI-guided in vivo optical imaging using Receiver Operating Characteristic analysis.

Reportable outcomes

The first year of this traineeship grant has led to one second author publication manuscript currently under review (Journal of Biomedical Optics), one second author paper in preparation, and one first author paper in preparation. In addition to attending seminars and conferences, I also served as a workshop instructor for the Workshop on Diffuse Optical Tomography: NIRFAST software using MATLAB at OSA Biomedical Optics (April 12-14, 2010), and an organizer and workshop instructor at the Image-Guided Spectroscopy Symposium and Workshop at the Thayer School of Engineering, Dartmouth College (July 19 - 23, 2010).

Conclusions

Substantial progress has been made on the numerical modeling and system development aspects of the project. Three dimensional modeling of tumors in excised tissue has been accomplished and the introduction of spectral resolution in the imaging strategy shows promise for quantifying tumor depth in the tissue. A prototype imaging system has been developed for intra-surgical margin detection with initial studies demonstrating the potential to determine the depth of embedded tumor fragments in the excise tissue or surgical cavity. Pilot animal data with the Licor IRDye800CW-2DG optical probe in MDA231 tumors showed poor specificity and tumor penetration. These results are not promising for diagnosing tumor margins with this fluorescent compound; however, further investigation with this probe is ongoing. While the animal experiments have progressed at a slower pace than originally proposed, I have received substantial training in this area and with 40 animals currently growing xenograft tumors in the mammary fat pad, the pace of experiments will increase sharply within the next 1 – 2 months. These studies will also involve the trastuzumab-bound NIR fluorophore which is expected to provide higher specificity between tumor and normal tissue in the HER-2 positive tumor line. Finally, ROC analysis was used to quantify imaging performance of an in vivo MRI-coupled diffuse tomography imaging system and these data are being prepared for publication.

References

1. S. C. Davis, B. W. Pogue, S. B. Tuttle, H. Dehghani, K. D. Paulsen, *Applied Physics (in press)*, (2008).
2. J. Svensson, S. Andersson-Engels, *Opt. Exp.* **13**, 4263 (2005).
3. J. Swartling, J. Svensson, D. Bengtsson, K. Terike, S. Andersson-Engels, *Appl. Opt.* **44**, 1934 (2005).

Appendix

The relevant journal article manuscript has been attached. This manuscript is under review.

Analytic expression of fluorescence-ratio detection correlates with depth in multi-spectral sub-surface imaging

Frederic Leblond
Thayer School of Engineering
Dartmouth College
8000 Cummings Hall
Hanover NH, 03755
Phone: 603-646-3056
Fax: 603-646-3856
Email: Frederic.Leblond@dartmouth .edu

Scott C. Davis
Thayer School of Engineering
Dartmouth College
8000 Cummings Hall
Hanover NH, 03755
Fax: 603-646-3856
Email: Scott.C.Davis@dartmouth.edu

Zaven Ovanesyan
Thayer School of Engineering
Dartmouth College
8000 Cummings Hall
Hanover NH, 03755
Fax: 603-646-3856
Email: Zaven.Ovanesyan@dartmouth.edu

Pablo A. Valdes
Thayer School of Engineering
Dartmouth College
8000 Cummings Hall
Hanover NH, 03755
Fax: 603-646-3856
Email: Pablo.A.Valdes@dartmouth.edu

Anthony Kim
Division of Biophysics and Bioimaging
Ontario Cancer Institute
610 University Avenue
Toronto ON, M5B 2K3
Phone: 416-946-4501
Fax: 416-946-6529
Email: anthonyk@uhnres.utoronto.ca

Venkataramanan Krishnaswamy

Thayer School of Engineering
Dartmouth College
8000 Cummings Hall
Hanover NH, 03755
Fax: 603-646-3856
Email: Venkataramanan.Krishnaswamy
@dartmouth.edu

Brian C. Wilson
Division of Biophysics and Bioimaging
Ontario Cancer Institute
610 University Avenue
Toronto ON, M5B 2K3
Phone: 416-946-4501 (x3683)
Fax: 416-946-6529
Email: wilson@uhnresearch.ca

Alex Hartov
Thayer School of Engineering
Dartmouth College
8000 Cummings Hall
Hanover NH, 03755
Fax: 603-646-3856
Email: Alexander.Hartov@dartmouth.edu

Brian W. Pogue
Thayer School of Engineering
Dartmouth College
8000 Cummings Hall
Hanover NH, 03755
Fax: 603-646-3856
Email: Brian.W.Pogue@dartmouth.edu

Keith D. Paulsen
Thayer School of Engineering
Dartmouth College
8000 Cummings Hall
Hanover NH, 03755
Fax: 603-646-3856
Email: Keith.D.Paulsen@dartmouth.edu

David W. Roberts
Section of Neurosurgery
Dartmouth Hitchcock Medical Center
One Medical Center Drive
Lebanon, NH, 03756
Phone: 603-650-8734
Fax: 603-650-7911
Email: David.W.Roberts@dartmouth.edu

Abstract: Analytical solutions to diffuse light transport in biological tissue are derived providing a closed form expression to estimate the depth of fluorescent molecules based on the spectral deformation of diffused near-infrared measurements. It is shown that the predicted depth is linearly related to the logarithm of the ratio of fluorescence at two different wavelengths, as long as the depth is beyond a few millimeters and the tissue is relatively homogenous. In agreement with theoretical predictions, experimental data, acquired on a tissue-simulating blood phantom with a broad-beam non-contact multi-spectral imaging system, is used to confirm that the ratio of fluorescence at two different wavelengths correlates with depth. Further elucidation of the relationship between depth and deformation of fluorescence spectra is provided by demonstrating that that the slope and intercept values of the relation between fluorescence ratio and depth is a function of tissue absorption and reduced scattering. Those findings are used as a basis for proposing that fluorescence contrast depth assessment can be achieved in fluorescence-guided neurosurgery allowing improved intra-operative delineation of tumor margins. In principle, this approach could also be applied in other preclinical or clinical imaging where luminescence contrast depth assessment is required in a multi-pixel sub-surface imaging geometry.

Keywords: fluorescence, multi-spectral imaging, diffusion theory, image-guided surgery, protoporphyrin IX, brain tumors

1 Introduction

Over the course of the last decade, there has been increased interest in the development of pre-clinical and clinical methods allowing tissue resection based on intra-operative fluorescence imaging. The motivation for this type of research is the application of optical methods in the operating room that provide surgeons with pertinent tissue information that is complementary to that conveyed by conventional white-light images. A clinical application of fluorescence-guided surgery that is becoming more widespread consists in the resection of brain tumors using the intrinsic metabolic and structural changes induced by the administration of δ-aminolevulenic acid (ALA). In this case, exogenous administration of ALA overloads the heme cellular pathway leading to selective accumulation of the fluorescent heme precursor, protoporphyrin IX (PpIX), in neoplastic tissues. Accumulated levels of PpIX in abnormal tissues are sufficiently high that certain types of tumors can be visualized through a surgical microscope modified with a fluorescence imaging channel [1, 2].

The current state-of-the-art methodology for fluorescence-guided brain tumor resection consists in using a modified surgical microscope to excite the PpIX molecules using a broad-beam blue light source. Photodetection of the re-emitted fluorescence is then achieved using a charged-coupled device (CCD) camera coupled to a high-pass filter [3]. However, an inherent limitation of this *in vivo* fluorescence imaging method is the strong light absorption in the visible part of the electromagnetic spectrum, typically making measurements sensitive only to biological events occurring within a few layers of cells. Therefore, the current state-of-the-art for fluorescence-guided resection is severely limited in its ability to identify sub-surface tumor remnants. Light in the NIR,

however, can travel much deeper into tissue because there tissue absorption decreases by two to three orders of magnitude, when compared to visible light. In the NIR range, scattering becomes the dominant light attenuation mechanism. Despite the resulting increased depth sensitivity however, planar epi-illumination NIR images are difficult to interpret because the information they convey is surface-weighted with a strong bias toward fluorescence near the surface [4].

Moving beyond simple planar images by providing surgeons with complementary information relating to the depth of fluorescent sources is an important aspect of future developments in fluorescence-guided surgery. A possibility, when it comes to retrieving depth information, consists in developing an intra-operative diffuse fluorescence tomography instrument. Such a method would involve a laser beam scanned across the region-of-interest (ROI) on the tissue surface. For each illumination point, a CCD image would be acquired providing a high density of measurements tomography dataset [5, 6]. Given proper light transport modeling can be achieved, an inverse problem would then be solved providing the surgeon with intra-operative tomography images with tissue information up to 1-2 cm underneath the surface of the surgical cavity. However, there are several impediments to the integration of such an approach in neurosurgery. In order to be practical, a depth-resolved approach should be implemented in such a way that the surgical workflow is minimally disturbed. From that point of view, intra-operative diffuse fluorescence tomography might not be an optimal choice because of the large time required to acquire a full dataset with acceptable signal-to-noise characteristics, as well as the potentially large time required to actually reconstruct and properly analyze the tomography images.

This paper presents preliminary results in the development of a depth-resolved fluorescence imaging approach compatible with the neurosurgical workflow. The proposed methodology is a novel non-tomographic approach potentially allowing pixel-by-pixel fluorophore depth estimation to be obtained at an imaging rate that is sufficiently close to real-time and that introduces minimal computational burden. The proposed methodology consists in acquiring two fluorescence images at different wavelengths and using their ratio to estimate the depth associated with the sources of fluorescence located underneath the tissue surface. Studies have shown that computational depth estimation based on multi-spectral data is feasible [7, 8]. However, the results derived from those studies are mainly applicable to contact point fluorescence measurements using fiber-optics, an approach that is not compatible with routine use in the scope of fluorescence-guided surgical applications. In comparison, the developments presented here provide evidence that analytical solutions to diffuse light transport can be used to estimate depth using a non-contact imaging system. Moreover, the depth-retrieval formalism developed here is argued to be amenable to wide-field CCD-based photo-detection in a manner that is compatible with the surgical workflow. On a more conceptual level, the work presented here fills a gap in the literature by providing closed form expressions from which the relation between spectral deformations, depth of fluorophores and intrinsic optical properties can be formally understood.

2 Methods and Results

2.1 The relationship between fluorescence ratio and depth

An example of a non-contact configuration for intra-operative multi-spectral imaging is illustrated in Fig. 1(a) where the optical light paths can be made compatible with those of existing surgical microscopes. In this configuration, the fluorescence excitation is generated using a broad-beam source in the NIR at the excitation wavelength, λ^{ex}. Remitted fluorescence signals are measured at two wavelengths, $\lambda_{1,2}>\lambda^{ex}$, in the fluorescence emission spectrum using band-pass filters and a cooled CCD chip. Assuming that tissue absorption due to the fluorophores is much smaller than that of other native chromophores (*e.g.*, oxy-hemoglobin, deoxy-hemoglobin) the light signals at each emission wavelength can be modeled using the expression

$$\psi^{em}(\vec{R},\lambda^{ex},\lambda) \approx Q_F \varepsilon_F^{em}(\lambda) \int_{\Omega} d^3 r\, \psi^{ex}(\vec{r}) C_F(\vec{r}) G^{em}(\vec{R},\vec{r},\delta^{\lambda},D^{\lambda}), \quad (1)$$

where Q_F is the quantum yield, $\varepsilon_F^{em}(\lambda)$ the emission spectrum and $C_F(\mathbf{r})$ the concentration of fluorophores at location **r**. Fig. 1(b) shows the main geometrical variables used in Eq. (1), in which light transport is modeled as a diffusive process. The fluence function ψ^{ex} is the excitation light field and G^{em} is the diffusion equation Green's function, which corresponds to the radiant exposure in response to a light impulse at **r**. For boundary conditions associated with an infinite homogenous medium, it is given by

$$G_{\infty}^{em}(\vec{R},\vec{r},\delta^{\lambda},D^{\lambda}) = \frac{\exp(-|\vec{R}-\vec{r}|/\delta^{\lambda})}{4\pi D^{\lambda}|\vec{R}-\vec{r}|}, \quad (2)$$

where the diffusion constant is $D^{\lambda} = 1/3\left(\mu_a^{\lambda} + \mu_s^{'\lambda}\right)$ and the penetration depth is $\delta^{\lambda} = \sqrt{D^{\lambda}/\mu_a^{\lambda}}$ [9].

A closed form expression is now derived from which a depth value can be attributed to each point imaged on the tissue surface. This is performed making the approximation that all of the fluorescence emanating from the surface is from a point-like distribution with molar concentration C_F at $\mathbf{r}_s$. This is equivalent to setting $C_F(\vec{r}) = C_F\delta^{(3)}(\vec{r} - \vec{r}_s)$ in Eq. (1), which then takes the form

$$\psi^{em}(\vec{R}, \lambda^{ex}, \lambda) \approx C_F Q_F \varepsilon_F^{em}(\lambda)\, \psi^{ex}(\vec{r}_s)\, G^{em}(|\vec{R} - \vec{r}_s|, \delta^{\lambda}, D^{\lambda}), \quad (3)$$

where the depth of the distribution is $|\vec{R} - \vec{r}_s| = d$ (*l*=0 mm in Fig. 1(b)). To illustrate how fluorescence spectra are affected by varying the depth of the fluorophore distribution, Fig. 2(a) shows PpIX spectra computed with Eq. (3) for depths varying up to *d*=20 mm for the absorption spectrum labeled *spectrum 1* in Fig. 3 and a constant value of reduced scattering (μ_s'=1 mm^{-1}). As the object gets deeper in the tissue, the optical properties demonstrate an increasing influence on shaping the spectrum because of the increasing pathlengths traversed by light. The information contained in the distorted spectra may be distilled into a single quantity by calculating the ratio of the signal at two emission wavelengths,

$$\Gamma = \frac{\psi^{em}(\vec{R}, \lambda^{ex}, \lambda_1)}{\psi^{em}(\vec{R}, \lambda^{ex}, \lambda_2)} \times \frac{\varepsilon_F^{em}(\lambda_2)}{\varepsilon_F^{em}(\lambda_1)} = \frac{G^{em}(\vec{R}, \vec{r}_s, \delta^{\lambda_1}, D^{\lambda_1})}{G^{em}(\vec{R}, \vec{r}_s, \delta^{\lambda_2}, D^{\lambda_2})}, \quad (4)$$

where the intensity values at each wavelength are normalized with the relative signal strength of an undistorted emission spectrum (e.g., spectrum labeled *0 mm* in Fig. 2a) implying that Γ should be equal to 1 for *d*=0 mm. Normalization with the reference spectrum allows direct comparison between ratios computed with Eq. (4) and experimental data acquired with a multi-spectral instrument. A critical aspect of Eq. (4) is that Γ is independent of the diffuse excitation field. This means that, in the point-source approximation limit, the ratio is independent of the manner with which the imaging field is illuminated. Therefore, assuming that the point approximation is valid (see comments addressing this approximation in Section 3), the equations presented here are valid for cases where the surgical filed is illuminated with a broad-beam source. Inserting Eq. (2) into Eq. (4), we find that the logarithm of the fluorescence ratio for an infinite medium is linearly related to the depth of the fluorophores with a slope equal to the difference in penetration depth between wavelengths λ_1 and λ_2,

$$\ln \Gamma_\infty = -\left[\frac{1}{\delta^{\lambda_1}} - \frac{1}{\delta^{\lambda_2}}\right] \times d + \ln \frac{D^{\lambda_2}}{D^{\lambda_1}}. \qquad (5)$$

This simple linear relationship suggests that depth can be estimated from a simple measured ratio provided the optical properties (absorption, scattering) of the tissue at the two wavelengths are known. Also of importance here is the fact that this expression provides a theoretical basis for interpreting the experimental and simulation results presented in Refs [7, 8]. However, the underlying photon diffusion assumptions used to derive Eq. (5) restrict its application to depths for which the diffusion approximation

applies, *i.e.*, for objects located more than 1 to 2 mm underneath the surface. This limitation is manifest in Eq. (5) by considering the *d*=0 mm limit, which yields $\Gamma_\infty \neq 1$.

In deriving Eq. (5) two assumptions were made that could potentially introduce errors in depth estimation, namely the medium was assumed to be homogeneous and of infinite spatial extent. While quantifying the effects of tissue heterogeneity on depth recovery is difficult and likely to vary for different tissue types, experience gained in diffuse optical fluorescence tomography has shown that using ratios of light signals that have sampled the same tissue volumes decreases the impact of heterogeneities and light coupling in and out of the tissue. In other contexts, normalization schemes have been used to bring tomography datasets closer to a form where they can be treated as if they had been obtained by interrogating a homogenous medium [10]. With respect to boundary conditions, the treatment for the infinite case can easily be extended to a more realistic semi-infinite geometry which more closely represents a surgical imaging configuration, as shown in Fig. 1(b). In this case, the diffusion equation is solved ensuring that the fluence vanishes on a planar extrapolated boundary located a distance $z_b^\lambda = 2AD^\lambda$ (A≈3 for air-tissue interface) away from the tissue surface [11]. The corresponding Green's function is then

$$G_{1/2}^{em}(\vec{R},\vec{r}_s,\delta^\lambda,D^\lambda) = \frac{1}{4\pi D^\lambda}\left[\frac{\exp(-|\vec{R}-\vec{r}_s|/\delta^\lambda)}{|\vec{R}-\vec{r}_s|} - \frac{\exp(-|\vec{R}-\vec{r}_{im}|/\delta^\lambda)}{|\vec{R}-\vec{r}_{im}|}\right], \qquad (6)$$

where, for *l*=0 mm, the distance between the measurement point and the imaginary negative source is given by $|\vec{R}-\vec{r}^{\,im}|=d+2z_b^{\lambda}$. The expression for the ratio of fluorescence becomes

$$\Gamma_{1/2}=\Gamma_{\infty}\times\left\{1-\left(\frac{1}{1+\frac{4AD^{\lambda_1}}{d}}\right)\exp\left(-\frac{4AD^{\lambda_1}}{\delta^{\lambda_1}}\right)\Big/\,1-\left(\frac{1}{1+\frac{4AD^{\lambda_2}}{d}}\right)\exp\left(-\frac{4AD^{\lambda_2}}{\delta^{\lambda_2}}\right)\right\}, \qquad (7)$$

where the second term in the brackets can be interpreted as a form factor correction to the expression obtained for an infinite medium. Compared with Eq. (5), the semi-infinite expression would slightly complicate the depth retrieval procedure, since the correction factor depends explicitly on the depth, which would require the use of iterative numerical resolution methods. However, it should be noted that the form factor becomes independent of depth for values that are significantly larger than $d_c=4AD^{\lambda}$. For example $d_c\approx 2$ mm for tissue with reduced scattering values of $\mu_s'=2$ mm^{-1}. This implies that for large enough depths the linear relationship in Eq. (5) is retrieved up to a depth-independent scaling factor dependent on the tissue properties δ^{λ} and D^{λ}.

2.2 Expected variations of measured fluorescence ratio with depth

As evidenced by the expressions for the slope in Eq. (5) and the form factor in Eq. (7), a critical ingredient in the accurate estimation of depth consists in the availability of prior knowledge relating to tissue optical properties (i.e., absorption and scattering parameters) at wavelengths for which fluorescence signals are acquired. Moreover,

initial assessment of whether or not fluorescence ratio measurements can be used for depth retrieval depends on whether or not measurable signal changes with depth can be detected for optical properties that are typically encountered for *in vivo* imaging applications. In order to emphasize this, Fig. 4(a) shows the fluorescence ratio (λ_1=650 nm and λ_2=670 nm) as a function of depth for the three representative absorption spectra shown in Fig. 3. It should be noted that those spectra were computed based on hyper-spectral reflectance data acquired *in vivo* with a hand-held fiber-optics probe by interrogating human brain tissue as part of a pilot clinical study involved 12 patients undergoing brain tumor resection procedures (See Ref. [12] for details relating to this intra-operative instrument as well as light transport-based algorithms used to retrieve the absorption and reduced scattering coefficients). As shown in Fig. 4(a), the curve for which the difference in inverse penetration depth is the smallest (top curve) is associated with a Γ-d relationship which is approximately linear. This can be explained by considering the linear limit of Eq. (5), *i.e*., by Taylor expanding and assuming the penetration depth difference is small. This finding is the explanation behind the observation made in Refs. [7, 8] that the relation between Γ and depth is linear.

Equation (5) also indicates that the choice of wavelengths used in the ratio affects the sensitivity of Γ to depth. Ideally, the chosen wavelengths should have dramatically different optical properties to emphasize the spectral distortion, which will be manifested as a steeper slope in the Γ-d relationship. An initial assessment of this can be achieved by considering the linear limit of Eq. (5) showing that the percentage of Γ-signal change per mm of increased depth is approximately $-\sqrt{3}\left(\sqrt{\mu_a^{\lambda_1}\mu'^{\lambda_1}_s}-\sqrt{\mu_a^{\lambda_2}\mu'^{\lambda_2}_s}\right)\times 100\%$, for $\mu'_s \gg \mu_a$. This implies that depth computation is

facilitated when the difference in optical properties is maximized. However, under similar light illumination conditions, tissue that is more absorbing will lead to fluorescence measurements with smaller signal-to-noise ratio making it more difficult to detect at larger depths. As an example of the signal variations that can be expected *in vivo*, optical property values derived from the spectra shown in Fig. 3 can be used to estimate the expected levels of signal variations with depth. For example, if μ_s'=1 mm^{-1} and $\mu_a^{\lambda 1}$ = 0.06 mm^{-1}, absorption changes of $\Delta\mu_a = \mu_a^{\lambda 1} - \mu_a^{\lambda 2}$ = 0.001 mm^{-1}, $\Delta\mu_a$ = 0.01 mm^{-1} and $\Delta\mu_a$ = 0.05 mm^{-1} lead to detected ratio changes of 0.4%, 3.7% and 25.1% per mm, respectively. These variations further demonstrate that the choice of wavelengths used can dramatically affect the sensitivity of Γ to depth as well as the permissible level of noise in the signal. Inspection of Fig. 3 shows that observed spectral variations for brain tissue should provide an opportunity to generate significant variations allowing signals from different depths to be discriminated. Noteworthy is the large variability of intra-operative normal brain absorption coefficient values, i.e., μ_a = 0.12 mm^{-1} to μ_a = 0.005 mm^{-1} across the spectral acquisition domain ranging from 630 nm to 730 nm. Further, to illustrate how fluorescence spectra are affected by varying the depth of the fluorophores, Fig. 2(a) shows normalized simulated PpIX spectra computed with Eq. (3) for various depths for the absorption spectrum labeled *spectrum 1* in Fig. 3 (μ_s' = 1 mm^{-1}). At increasing depths, simulations show the influence of tissue optical properties on the spectrum and its subsequent deformation due to the different light paths traversed.

An important point that the analytical work presented here is emphasizing is that depth retrieval based on multi-spectral fluorescence data requires absorption and scattering properties of the interrogated tissue to be known *a priori*. However, in a

context where optical data is acquired *in vivo* during surgery, implementing a method through which the endogenous optical properties are determined in real time might not always be feasible. Therefore, it is important to understand how sensitive depth estimation is to optical properties errors in order to better assess the required precision. As an initial assessment, the algorithm presented above was used to retrieve depth using incorrect values of optical properties. To that effect, Fig. 4(b) shows curves illustrating the impact of using the wrong optical properties when using Eq. (5) to retrieve depth. For the two cases shown (top and bottom curves), the true optical properties were assumed to match those of *spectrum 1* in Fig. 3. Using slopes and intercepts derived from Eq. (5) for λ_1=650 nm and λ_2=670 nm, values of depth were recovered using the incorrect properties from *spectrum 2* (top curve) and *spectrum 3* (bottom curve). Clearly, using the wrong optical properties can lead to depth estimation errors of several millimeters, the magnitude of which increases with depth. The strong reliance on the accurate tissue properties suggests that this approach should be implemented with supplemental capabilities to simultaneously determine the optical properties of the tissue in the imaging field. In principle this can be accomplished with a system similar to that shown in Fig. 1(a) where multi-spectral or hyper-spectral NIR transmission data is acquired and fitted for absorption and scattering spectra against light transport solutions of the form shown in Eq. (6). A simpler approach would consist in using the fibers-optics probe described in Ref. [12] to estimate the bulk values of the tissue optical properties in the surgical cavity prior to imaging using the wide-field multi-spectral instrument.

2.3 Preliminary experimental evaluation

An initial experimental assessment of the proposed imaging method has been performed by designing an instrument (see schematics in Fig. 1(a)) for wide-field acquisition of multi-spectral measurements. Fluorescence excitation is done using the expanded beam of a diode laser with wavelength λ^{ex} = 635 nm (Power Technology Inc., Little Rock, Arkansas). Remitted fluorescence is measured at five wavelengths, λ = (675, 685, 695, 705, 715) nm, using 10 nm-wide band-pass interference filters (Omega Optical, Brattleboro, Vermont) inserted into a motorized wheel coupled to an EXi Aqua charge-coupled device (CCD) (QImaging, Surrey, British Columbia). The camera is cooled at 0°C and has a full well-depth of 18,000 e-, a 14 bits digitizer, a dark current of 0.15 e-/pixel/seconds and a read-noise of 6.5 e- when operated at 10MHz readout frequency.

The proposed methodology was then evaluated by imaging a tissue-simulating blood phantom. A container (dimensions: 150 mm $\times$ 75 mm $\times$ 61 mm) was filled with water containing a volume fraction of 1% intralipid (Baxter Healthcare Corp., Deerfield, Illinois) and 2% porcine blood. An optically transparent cylindrical inclusion (diameter: 5.5 mm, height: 10 mm) was filled with 20 μg/ml of PpIX (Frontier Scientific, Logan, Utah) dissolved in dimethyl sulfoxide (DMSO). A moving stage allowed the inclusion to be immersed at different depths. Fig. 5(a) shows the optical properties of the medium computed using the fiber-optics probe described in Ref. [12]. The medium was illuminated using an expanded laser beam (diameter: 13 mm, P = 5.5 mW, λ^{ex} = 635 nm). Fluorescence images at five different wavelengths were acquired (d = 1 to 15 mm). A PpIX spectrum was acquired to be used as a reference that has not been corrupted

by light propagation in the medium. Associated with each fluorescence image, a pre-contrast image (inclusion filled with DMSO only) was acquired and subtracted from the corresponding image to account for excitation light filter bleed-through. For all depths, the characteristic shape of the NIR PpIX shoulder was retrieved up to deformations caused by diffusion, as shown in Fig. 2(b). Fig. 5(b) shows the measured ratios for two sets of wavelengths: (λ_1, λ_2) = (675 nm, 685 nm) (circles) and (λ_1, λ_2) = (675 nm, 695 nm) (squares). The dotted lines correspond to simulated ratios computed with Eq. (6) using the optical properties experimentally retrieved with the fiber-optics probe (Fig. 5(a)). Qualitative inspection of the data suggests a reasonable match between theory and experiment, although a significant level of noise is observed mainly due to excitation light filter bleed-through, limited light power delivered to the tissue surface and variations of the optical properties of the blood phantom during the experiment (as much as 20% for the absorption coefficient). Using a (non-parametric) Spearman's rank correlation test a significant correlation was found between the experimental data and the theoretical predictions. The correlation coefficients and P-values obtained were r_s = 0.90, P = 0.0046 (two-tailed) for (λ_1, λ_2) = (675 nm, 685 nm) and r_s = 0.83, P = 0.015 (two-tailed) for (λ_1, λ_2) = (675 nm, 695 nm). A linear regression was performed on the data with goodness-of-fit parameters r^2 = 0.84 and r^2 = 0.64 for (λ_1, λ_2) = (675 nm, 685 nm) and (λ_1, λ_2) = (675 nm, 695 nm), respectively. Another statistical analysis (F-test) was performed to test for the presence of a non-zero slope in the relationship between Γ and *d*. We found that for both sets of wavelengths the data was significantly different from a horizontal line (P<0.05).

4 Discussion

Current methodology for brain tumor resection involves the use of pre-operative magnetic resonance (MR) images co-registered with the surgical field, which is viewed by the surgeon through a conventional surgical microscope. More recently, intra-operative fluorescence microscopes have been used providing surgeons with more accurate tumor detection capabilities when used in conjunction with the precursor molecule ALA. However, for a large number of cases it is suspected that even when a lesion has been *fully* resected based on MR contrast, trained visual inspection, and visible fluorescence, residual tumor remnants are left behind underneath the surface of the cavity. Any information that is provided beyond what is currently seen using state-of-the-art fluorescence surgical microscopes is therefore likely to be perceived as a major advance in neurosurgery. Given the current state-of-the-art for fluorescence-guided resection of brain tumors (using blue light excitation) can only detect on the surface of the cavity, routine detection and localization of tumors at 1-2 cm depth with NIR light should lead to significant patient benefits in terms of improved quality of life and survival. Within the limits of the approximations that were used in the derivation, the simple relationships Eq. (5) and Eq. (6) between fluorophore depth and fluorescence ratios at two wavelengths suggest that a methodology could be implemented allowing intra-operative estimation of residual tumor depth using non-contact fluorescence imaging microscopes. However, the relationship between d and Γ depends explicitly on the optical properties at the measurement wavelengths, so a challenge for this type of approach is that is must be implemented alongside an independent tissue characterization technique.

Another potential limitation of the approach is that the point-like approximation has been made in order to derive a simple Γ-d relationship from which depth could be retrieved with negligible computational burden when compared to, *e.g.*, the resolution of an inverse problem in diffuse fluorescence tomography. However, the analysis presented in section 2.3 supports the validity of this approximation by showing that there is a strong correlation between the theoretical model and experimental fluorescence ratio data. It should be clear though that depth retrieval based on this approximation will not be exact because the distribution of fluorescence emanating from tumors is clearly not point-like. In reality, the assumption that is made is that most of the fluorescence that is directly detected over the surface of tissue (l = 0 mm in Figure 1(b)) will emanate from molecular sources directly below the surface area where fluorescence is detected. As a consequence, on average the detected signal should be associated mostly with fluorophores in the tumor that are closest to the detection point. In reality of course, other parts of the tumor will contribute, so the depth that is actually retrieved from the signal will provide an approximate value, which in effect will be a weighted average of the depth from all contributing tumor areas. The required level of precision for fluorescence-guided surgery (as attested by contributing neurosurgeons) is such that the precision reached for depth prediction with fluorescence ratio measurements can be a few millimeters off. Full validation of the precision of the point-like approximation for depth retrieval will be achieved in future studies where an optimized instrument will be used in the scope of *in vivo* studies. It should also be noted that the point-like approximation has been used in published work before, such as in

Ref. [13] where time-domain data has been used to predict the depth of a fluorescent inclusion of finite spatial extent.

Because NIR light is exponentially attenuated in tissue (modified Beer-Lambert law), the information conveyed by epi-illumination imaging is surface weighted. Therefore, contributions coming from the auto-fluorescence of tissue can significantly diminish the ability to image deeply buried sources of fluorescence as well as significantly compromise the validity of the point-like approximation. However, the majority of auto-fluorescent endogenous molecules have excitation spectra in the visible part of the electromagnetic spectrum. Since the illumination with the proposed methodology is in the far-red part of the spectrum (λ_{ex} = 635 nm), auto-fluorescence is expected to be small when the method is used *in vivo*. Moreover, an oftentimes dominating source of tissue auto-fluorescence is the skin. However, in the brain tumor resection application that is presented in this manuscript, skin is not an issue because fluorescence imaging is performed intra-operatively after cranium opening [14]. Perhaps more convincing in addressing the issue of auto-fluroescence however, is the fact that the level of ALA-induced PpIX fluorescence from brain tumors (including high- and low-grade gliomas, meningiomas and metastasis) is two to three orders of magnitude larger when compared to normal adjacent brain tissue. The high specificity of this contrast mechanism is such that fluorescence emanating from areas other than the tumor is in the vast majority of cases negligible [15].

Therefore it is expected that the validity of the point-like approximation will not be compromised by the presence of auto-fluorescence and non-specific fluorescence for such clinical applications as the resection of brain tumors based on ALA-induced PpIX

fluorescence. Moreover, the preliminary results presented in this work show that fluorophore depth correlates with measured fluorescence ratios despite the fact several approximations were made in deriving the analytic light transport solutions. This provides strong evidence that a non-contact broad-beam fluorescence imaging approach can be implemented and used intra-operatively in order to estimate the depth of fluorescence lesions in a manner that is minimally disruptive to the surgical workflow. However, using a depth retrieval algorithm based on Eq. (6) with the fluorescence-ratio data presented in Fig. 5(b) leads to depths errors which can only be minimized through instrument modifications reducing the level of noise in the data. Future work will be concerned with those issues to be addressed by developing an imager using a light source with increased power as well as light filtering components minimizing excitation light filter bleed-through. Significant improvements in signal-to-noise characteristics for the fluorescence ratios are expected allowing depth to be retrieved from the measurements. Further validation of the approach will be conducted by integrating multi-spectral measurements into the neurosurgical tumor resection workflow allowing for an actual assessment of the *in vivo* level of signal available as well as the development of algorithms optimizing the choice of wavelengths insuring maximization of fluorescence-ratio variations with depth. Estimation of tissue optical properties (absorption and scattering at the measured wavelengths) will be achieved by using the hand-held fiber-optics probe that is currently used in the scope of a brain tumor resection clinical study. The work presented in this letter is the first step towards the development of a method that can be readily applied to localize sub-surface pathologies

during wide-field intra-surgical fluorescence imaging, facilitating more complete tumor resections.

Acknowledgments

This work was supported by the National Institutes of Health (NIH) through Award Number K25CA138578 from the National Cancer Institute (NCI), NIH Grant Number R01NS052274-01A2 and Department of Defense Breast Cancer post-doctoral fellowship BC087754.

References

1. Stummer, W., et al., *Intraoperative detection of malignant gliomas by 5-aminolevulinic acid-induced porphyrin fluorescence.* Neurosurgery, 1998. **42**(3): p. 518-25; discussion 525-6.
2. Stummer, W., et al., *Fluorescence-guided surgery with 5-aminolevulinic acid for resection of malignant glioma: a randomised controlled multicentre phase III trial.* Lancet Oncol, 2006. **7**(5): p. 392-401.
3. Stummer, W., et al., *Technical principles for protoporphyrin-IX-fluorescence guided microsurgical resection of malignant glioma tissue.* Acta Neurochir (Wien), 1998. **140**(10): p. 995-1000.
4. Leblond, F., et al., *Pre-clinical whole-body fluorescence imaging: Review of instruments, methods and applications.* J Photochem Photobiol B, 2010. **98**(1): p. 77-94.
5. Kepshire, D.S., et al., *Subsurface diffuse optical tomography can localize absorber and fluorescent objects but recovered image sensitivity is nonlinear with depth.* Appl Opt, 2007. **46**(10): p. 1669-78.
6. Kepshire, D., et al., *Fluorescence tomography characterization for sub-surface imaging with protoporphyrin IX.* Opt Express, 2008. **16**(12): p. 8581-93.
7. Swartling, J., et al., *Fluorescence spectra provide information on the depth of fluorescent lesions in tissue.* Appl Opt, 2005. **44**(10): p. 1934-41.
8. Svensson, J. and S. Andersson-Engels, *Modeling of spectral changes for depth localization of fluorescent inclusion.* Opt Express, 2005. **13**(11): p. 4263-74.
9. Jacques, S.L. and B.W. Pogue, *Tutorial on diffuse light transport.* J Biomed Opt, 2008. **13**(4): p. 041302.
10. Ntziachristos, V. and R. Weissleder, *Experimental three-dimensional fluorescence reconstruction of diffuse media by use of a normalized Born approximation.* Opt Lett, 2001. **26**(12): p. 893-5.
11. Haskell, R.C., et al., *Boundary conditions for the diffusion equation in radiative transfer.* J Opt Soc Am A Opt Image Sci Vis, 1994. **11**(10): p. 2727-41.
12. Kim, A., et al., *A fiberoptic reflectance probe with multiple source-collector separations to increase the dynamic range of derived tissue optical absorption and scattering coefficients.* Opt Express, 2010. **18**(6): p. 5580-94.

13. Hall, D., et al., *Simple time-domain optical method for estimating the depth and concentration of a fluorescent inclusion in a turbid medium.* Opt Lett, 2004. **29**(19): p. 2258-60.
14. Roberts, D.W., et al., *Coregistered fluorescence-enhanced tumor resection of malignant glioma: relationships between delta-aminolevulinic acid-induced protoporphyrin IX fluorescence, magnetic resonance imaging enhancement, and neuropathological parameters.* J Neurosurg, 2010(April 9).
15. Valdes, P.A., et al., *Quantitative fluorescence concentration measurements in intracranial tumors: implications for PpIX as a surgical biomarker to guide resection procedures.* under review, 2010.

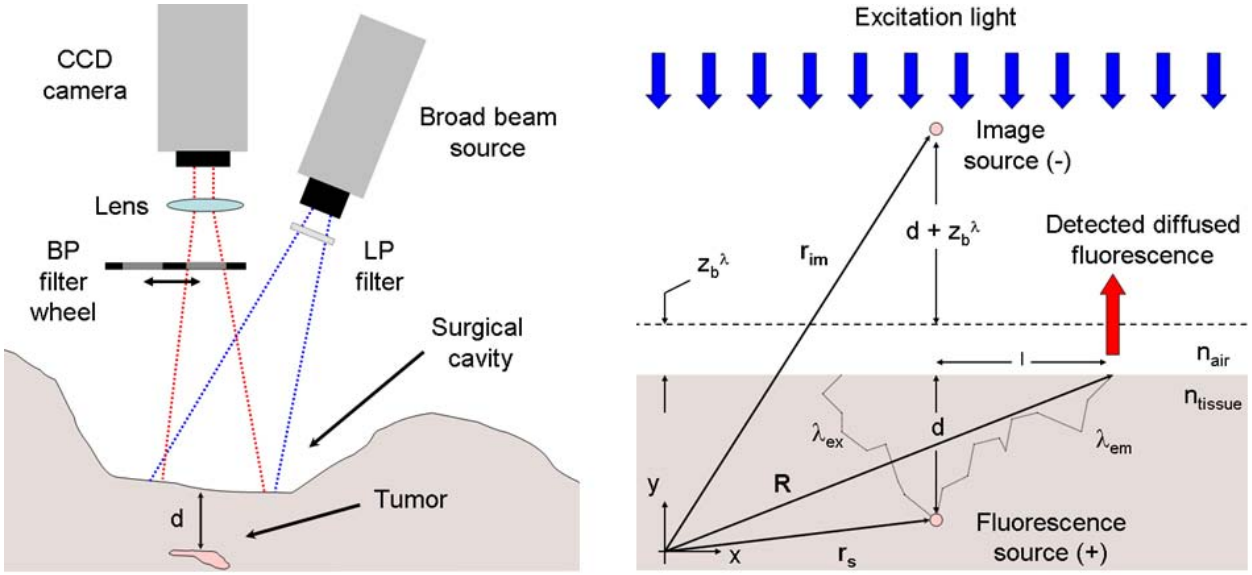

Fig. 1 (a) Non-contact multi-spectral imaging instrument used for fluorescence-ratio detection. (b) Light transport is modeled assuming the cavity can be approximated as a semi-infinite diffusive medium with homogeneous optical properties.

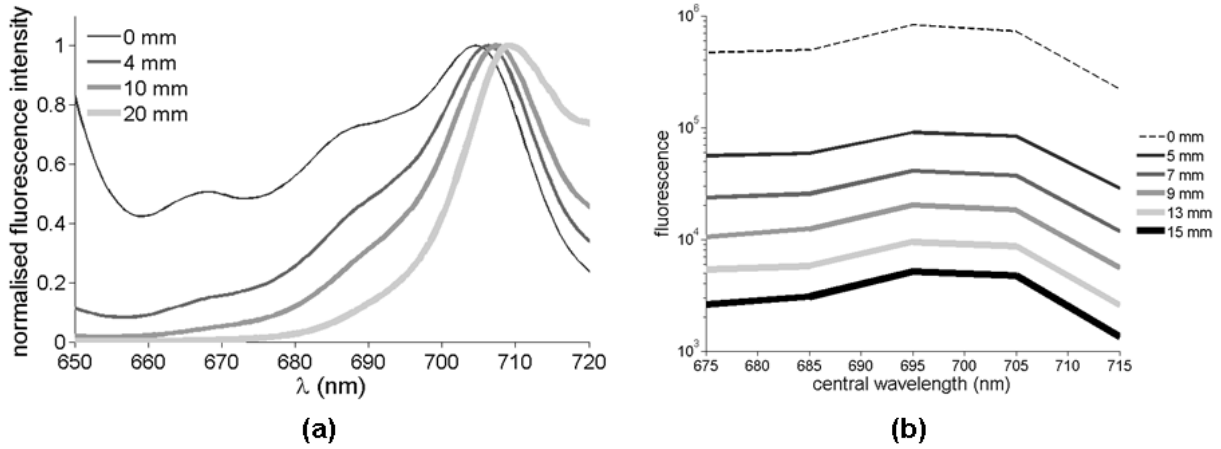

Fig. 2 (a) Simulation results showing PpIX spectra for molecules located at four different tissue depths. (b) Experimental spectra measured for a tissue-simulating blood phantom. The PpIX spectra shown are for different depths ranging from *d*=5 mm to *d*=15mm. The curve labeled *0 mm* is the reference spectrum acquired with a multi-spectral non-contact instrument.

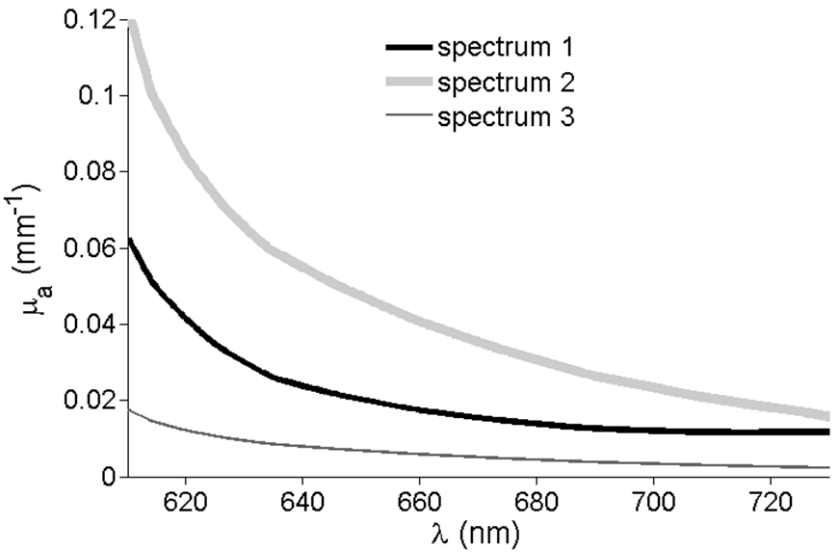

Fig. 3 Absorption spectra acquired *in vivo* for normal human brain tissue using a hyper-spectral hand-held fiber-optics probe.

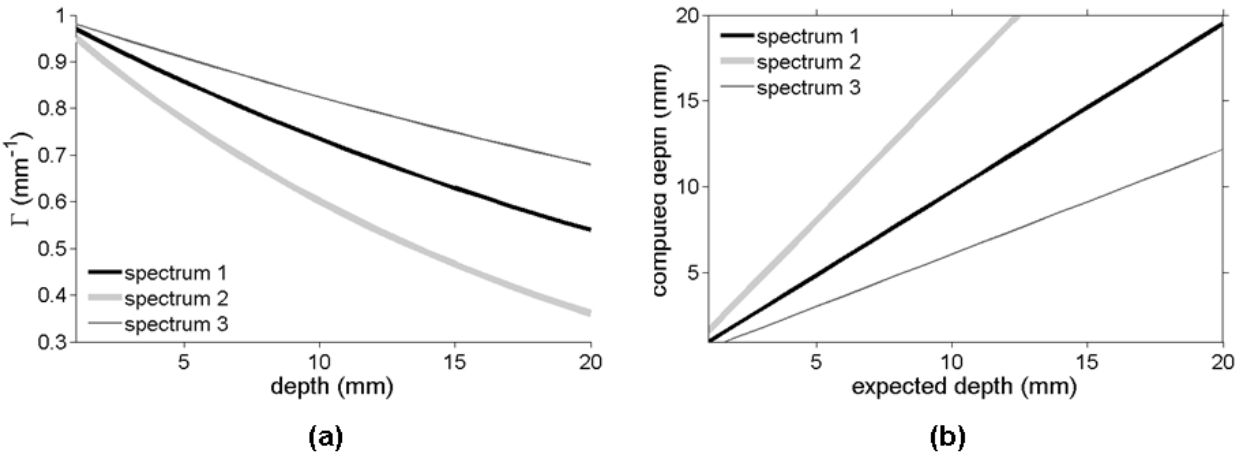

Fig. 4 (a) Γ as a function of depth for the three absorption spectra shown in Fig. 3, (b) Expected versus computed depth for different absorption spectra. The curves labeled *spectrum 2* and *spectrum 3* were computed using Eq. (5) assuming that the optical properties were those associated with *spectrum 1*. Deviations with respect to the darker curve (*spectrum 1*) should be interpreted as depth errors.

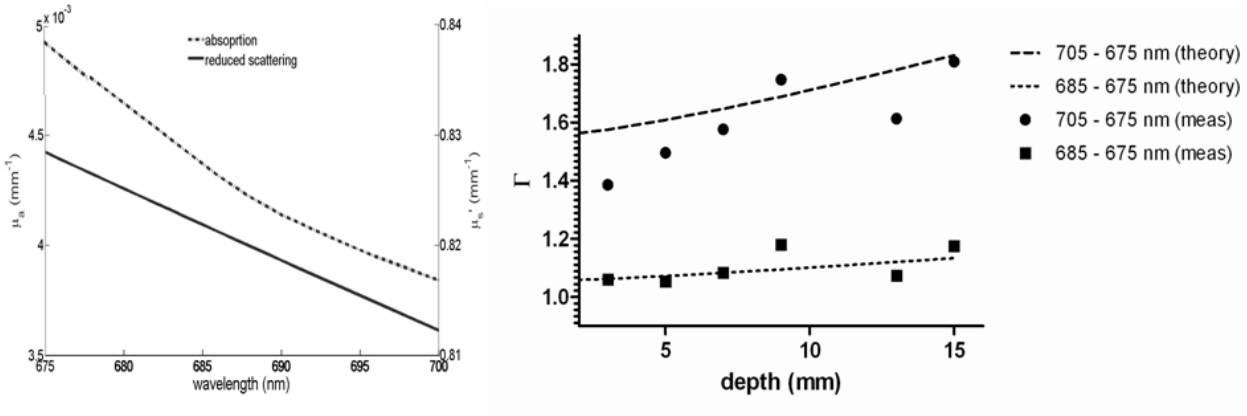

Fig. 5 Experimental data acquired using a tissue-simulating blood phantom: (e) Optical properties (absorption and reduced scattering) measured with the fiber-optics probe, (f) Simulated (theory) versus measured (meas) fluorescence ratios for two sets of wavelengths showing correlation with depth.